

**Size and transparency influence diel vertical
migration patterns in copepods.**

Alex Barth^{*1}, Rod Johnson² and Joshua Stone¹

1. University of South Carolina, Biological Sciences, 700 Sumter St
401, Columbia, SC 29208
2. Bermuda Institute of Ocean Sciences, Bermuda GE 01, UK

² **0.1 Scientific Significance Statement**

³ **0.1.1 Study Novelty**

⁴ Diel Vertical Migration is a widespread phenomenon across marine and fresh-
⁵ water systems. The predator evasion hypothesis suggests that DVM occurs as
⁶ zooplankton attempt to escape visual predators. Yet, DVM itself is a costly
⁷ and risky behavior. Thus, DVM should only occur when visual risk is high.
⁸ Several studies have shown that copepod size influences the magnitude of DVM.
⁹ However, an individual's visual risk may include traits beyond simply size. In
¹⁰ this study, we utilize an in-situ imaging tool to reveal how copepod morpholog-
¹¹ ical traits influence DVM. Our findings show that both size and transparency
¹² influence DVM. We support this finding through rigorous statistical analyses
¹³ and state-of-the-art technology. This finding provides support for leading DVM
¹⁴ hypotheses and highlights that DVM is a complex behavior driven by multiple
¹⁵ copepod traits. Furthermore, this study represents a novel application of in-situ
¹⁶ imaging technology to address major hypotheses in biological oceanography.

¹⁷ **0.1.2 Applicability to L&O**

¹⁸ This study addresses diel vertical migration, an active, major research topic in
¹⁹ biological oceanography. Many studies published in L&O contribute to advanc-
²⁰ ing knowledge on DVM. In this paper, we provide strong evidence for both size
²¹ and transparency influencing DVM behavior. Additionally, we accomplished
²² this study using emerging technology and statistical analyses. This work builds
²³ on research published in L&O and will be broadly applicable to plankton ecol-

²⁴ ogists, biological oceanographers.

²⁵ AB and JS developed the study hypotheses. JS coordinated deployment and
²⁶ data management of the UVP. RJ facilitated data collection on cruises. AB
²⁷ led the analysis and preparation of the manuscript and figures. JS and RJ
²⁸ contributed to the manuscript draft. All authors approved the final submission.

²⁹ 1 Abstract

³⁰ Diel vertical migration (DVM) is a widespread phenomenon in aquatic environments.
³¹ The primary hypothesis explaining DVM is the visual predator evasion hypothesis,
³² which suggests that zooplankton migrate to deeper waters to avoid detection during daylight.
³³ However, visual risk also depends on a copepod's morphology. In this study, we investigate hypotheses related to morphology and DVM: (H1) size increases visual risk and will increase DVM depth and
³⁴ (H2) copepod transparency will reduce visual risk and thus reduce DVM depth.

³⁵ In-situ Copepod images were collected across several cruises in the Sargasso Sea
³⁶ using an Underwater Vision Profiler 5. Copepod morphology was characterized
³⁷ from these images and a dimension reduction approach. The results show a clear
³⁸ relationship in which larger copepods have a larger DVM signal. Darker cope-
³⁹ pods also have a larger DVM signal, however only amongst the largest group of
⁴⁰ copepods. This suggests multiple morphological traits influence copepod DVM
⁴¹ behavior.

⁴⁴ **2 Introduction**

⁴⁵ Diel vertical migration (DVM) is a wide spread phenomena with large conse-
⁴⁶ quences in ocean ecosystems. DVM is the process of pelagic organisms verti-
⁴⁷ cally moving in the water column on a daily basis, often travelling dozens to
⁴⁸ hundreds of meters (Bianchi and Mislan 2016). This large-scale event occurs
⁴⁹ across many taxa, from plankton to fish (Brierley 2014). However, DVM is
⁵⁰ particularly notable in zooplankton communities, whose migrations contribute
⁵¹ substantially to biogeochemical cycles (Steinberg and Landry 2017; Archibald
⁵² et al. 2019; Siegel et al. 2023). Zooplankton communities, largely dominated
⁵³ by copepods (Turner 2004), will feed in surface layers of the ocean at night then
⁵⁴ migrate into deeper waters during daytime. Through this movement, copepods
⁵⁵ actively transport carbon to depth. Additionally, Kelly et al. (2019) described
⁵⁶ zooplankton DVM to be a major component of mesopelagic food webs. Thus to
⁵⁷ understand pelagic food webs and nutrient cycles, it is critically important to
⁵⁸ understand the drivers of DVM.

⁵⁹ Predominantly, zooplankton DVM is the movement from deep waters at daytime
⁶⁰ to shallower waters at night (Hays 2003; Bianchi and Mislan 2016). The leading
⁶¹ explanation for this pattern is the predator-avoidance hypothesis (Bandara et al.
⁶² 2021). This hypothesis posits zooplankton evacuate the sunlit surface to evade
⁶³ visual predators then ascend at night to feed. However, the massive migration
⁶⁴ undertaken by these copepods is energetically expensive (Maas et al. 2018; Robi-
⁶⁵ son et al. 2020). Therefore, the visual predator evasion hypothesis implies that

66 DVM is a result of visual risk exceeding migration costs. However, a copepod's
67 visual risk to a visual predator depends on morphological features (Aksnes and
68 Utne 1997). Notably a copepod's size can increase visual detection. Several
69 studies have documented that copepod size influences DVM magnitude (Hays
70 et al. 1994; Aarflot et al. 2019). Presumably, a copepod's transparency will
71 also influence DVM. Hays et al. (1994) reported that pigmentation explained
72 variation in DVM frequency. However, few other studies have investigated this
73 at length. One barrier to studying a relationship between copepod morphology
74 and DVM is the difficulty of accurately recording traits.

75 In-situ imaging tools offer great potential to better describe copepod DVM. By
76 directly observing copepods, new insights into their behavior and traits can be
77 resolved (Ohman 2019). For example, Whitmore and Ohman (2021) used an
78 in-situ imaging device to describe a relationship between copepod abundance
79 with a particulate field rather than chlorophyll-a. Such findings are facilitated
80 by the fact imagery data records an individual's exact position. Additionally, a
81 copepod's true appearance can be documented whereas net-collected organisms
82 are often physically deformed or lacking color due to decomposition or preserva-
83 tion. Some studies have noted a copepod DVM with in-situ imagery data (Pan
84 et al. 2018; Whitmore and Ohman 2021). However, direct tests of DVM-related
85 hypotheses with such data have not been conducted.

86 In this study, we utilized in-situ imaging to evaluate how copepod morphologi-
87 cal traits influence patterns. We specifically test the hypotheses that, (H1) size
88 increases visual risk and will increase DVM magnitude and (H2) copepod trans-

89 parency will reduce visual risk and thus reduce DVM. If these morphologically
90 based hypotheses are true, then the larger and darker copepods will have the
91 largest DVM signals.

92 3 Methods

93 3.1 CTD profiles and UVP imaging of copepods

94 Data were collected aboard the R/V Atlantic Explorer in collaboration with the
95 Bermuda Atlantic Time-series Study (BATS) (Steinberg et al. 2001). In-situ
96 images of plankton were acquired using an Underwater Vision Profiler (UVP5)
97 (Picheral et al. 2010). The original sampling methodology and instrument
98 specification followed details described in Barth and Stone (2022). The UVP was
99 attached to the CTD rosette and deployed regularly on cruises to the Sargasso
100 Sea from June 2019 - December 2021. Typical monthly cruises included ~13
101 profiles with average descents to 1200m (Supplemental Figure 1). In this study,
102 we investigated general trends in DVM by pooling together casts across multiple
103 cruises. This approach is necessitated by the small sampling volume of the UVP
104 and low abundance of plankton which requires aggregation of data to resolve
105 trends (Barth and Stone 2022). While there was some variation between cruises
106 (Supplemental Figure 2), this oligotrophic system is relatively consistent across
107 seasons (Steinberg et al. 2001). Additionally, every cruise had an approximately
108 equal number of day and night casts. Profiles were assigned to be day or night
109 based on locally calculated nautical dawn and nautical dusk times using the R

110 package **suncalc** 0.5.1.

111 The UVP records images of large particles ($>600\mu\text{m}$ equivalent spherical diam-
112 eter, ESD). However, living particles are not reliably identifiable below $900\mu\text{m}$
113 (Barth and Stone 2022). All recorded images were processed using Zooprocess
114 (Gorsky et al. 2010), which provides several metrics related to size, grey value,
115 and shape complexity. These features were then used to automatically sort
116 images using Ecotaxa (Picheral et al.). All images were manually verified by
117 the same trained taxonomist. In total, 294,913 images were recorded. Of these,
118 85.2% were images of debris or artefacts. The smallest identified copepod was
119 0.940mm ESD and the largest was 5.904mm ESD. Across all casts, copepods
120 were the most common organism, composing 58.7% of all identified, living par-
121 ticles. In total, there were 4151 individual copepods images.

122 3.2 Morphological Grouping

123 Zooprocess measures and collects several morphologically relevant parameters.
124 To create relevant groups of copepods, a dimension reduction approach was
125 used. Similar methods have been successfully utilized to provide novel insights
126 to marine snow (Trudnowska et al. 2021), copepod dynamics in the Arctic
127 (Vilgrain et al. 2021), and temporal trends in phytoplankton communities (Son-
128 net et al. 2022). First, 18 morphologically relevant parameters were selected
129 to be included in a principal Components Analysis (PCA), following (Vilgrain
130 et al. 2021). Parameters can be described as relating to size (e.g. major axis,
131 feret diameter, ESD), grey intensity (e.g. mean grey value at 625nm wavelength

132 light), shape (e.g. elongation, symmetry), and shape complexity (e.g. fractal
133 dimension). The PCA was weighted by the volume sampled in a 1-m depth bin
134 for each observation. This approach provides a correction for the UVP's vari-
135 able descent speed which can cause duplicate imaging of individuals. While this
136 phenomena has a minor impact on overall results (Barth and Stone 2022), we
137 used the weighted approach to assure that no individual features were overrepre-
138 sented. All morphological descriptors were scaled and centered prior to inclusion
139 in the analysis. The model was constructed using the R package **FactoMineR**
140 2.7. principal components were deemed to be significant if their eigenvalues
141 were greater than 1. This approach yielded 4 PCs which described 87.3% of the
142 total variation in morphological parameters, with 34.5% and 26.5% in the first
143 two components respectively. This four principal component space provides a
144 “morphospace” to characterize copepods.

145 To address our morphology-DVM hypotheses, we constructed discrete morpho-
146 logical groups based on the first two principal components. Groups along each
147 of the principal components were defined as low (below 25th percentile), mid
148 (25th-75th percentile) and high (greater than 75th percentile). To address the
149 size-dependent hypothesis (H1), groups were assigned as low, mid, or high along
150 PC1. Then to assess if color/transparency was a secondary factor (H2), within
151 each PC1 group, PC2 groups were constructed as low, mid, or high. In total,
152 this created 9 groups (e.g. Low PC1-Low PC2, Low P1-mid PC2, etc).

153 **3.3 Copepod vertical structure & DVM**

154 **3.3.1 Vertical distribution of copepods**

155 Copepods in this system are well documented to undergo DVM (Steinberg et
156 al. 2000; Schnetzer and Steinberg 2002; Maas et al. 2018). However, there
157 have not been direct measurements of DVM with in-situ imaging data. First, to
158 assess which portion of the water column copepods were utilizing for DVM, we
159 visualized the average vertical structure. The concentrations of each morpholog-
160 ical group (based on PC1 and PC2) were calculated in 20m depth bins for each
161 UVP profile. Profiles were designated as either day or night. Then across all
162 day/night profiles, the mean concentration was calculated for each 20m depth
163 bin.

164 **3.3.2 Weighted mean depth variability**

165 Weighted mean depth (WMD) is a common metric to describe vertical structure
166 and DVM in zooplankton (Ohman et al. 2002; Ohman and Romagnan 2016;
167 Aarflot et al. 2019). However, with in-situ imagery, this approach presents a
168 few challenges. WMD cannot be calculated individually for each profile then
169 averaged because each profile had a different descent depth. Additionally, the
170 small and uneven sampling volume of the UVP can make single casts too vari-
171 able to reliably resolve abundance. Yet, understanding variation around the
172 WMD is necessary to compare DVM strength across groups. Here, we intro-
173 duce a depth-bin constrained bootstrap approach to define WMD with a 95%
174 confidence interval. To do this, the concentration of each group, was calculated

175 in 20m depth bins for each profile. Then all profiles were ‘pooled’, separately
 176 for day/night. This provides a distribution of concentrations in each depth-bin.
 177 However, due to the different descent speeds and depth of profiles, there are
 178 more observations of surface depth bins. Thus, traditional bootstrapping would
 179 bias estimate toward the surface as resampling would be more likely to draw
 180 a more-frequently observed surface bin. To avoid this, bootstrap samples were
 181 “bin-constrained” such that for each iteration, a random observation was drawn
 182 within each depth bin, then replaced for the next iteration. A maximum depth
 183 was set to 600m based on qualitative observations of vertical profiles. This ap-
 184 proach effectively created a random profile by resampling a concentration, $conc^*$,
 185 from each depth bin, d . For each iteration, the random constructed profile then
 186 was used to calculate a bootstrapped weighted mean depth, WMD^* . This was
 187 done for each morphological group, g , at each time of day, t (day/night).

$$WMD_{g,t}^* = \sum_i^{N=30} \frac{d_i(conc_{i,g,t}^*)}{\sum_i^{N=30} conc_{i,g,t}^*}$$

188 The distribution of $WMD_{g,t}^*$ then was used to calculate a bootstrapped mean
 189 and 95% confidence interval. The 95% CIs could be compared between times
 190 of day and morphological groups to assess the strength of DVM. Using PC1
 191 to assess size, the WMD was compared between the three PC1-groups by per-
 192 centile level. Then to assess the effect of transparency the WMD was compared
 193 between PC2-groups within each PC1-grouping. A larger signal of DVM would
 194 be evident by a clearly deeper (non-overlapping 95% CI) daytime WMD.

¹⁹⁵ **4 Results**

¹⁹⁶ **4.1 Morphological Groups**

¹⁹⁷ The PCA revealed four major axis of variability (Figure 1). The first axis (PC1,
¹⁹⁸ 34.23% of variability) was largely explained by increasing values related to size,
¹⁹⁹ such as perimeter (loading score = 0.927) and feret diameter (loading score =
²⁰⁰ 0.910). The second axis (PC2, 27.24% of variability) can be interpreted as a
²⁰¹ gradient of transparent to dark individuals. PC2 was largely anticorrelated with
²⁰² mean grey value (higher values indicate a more transparent individual) (loading
²⁰³ score = -0.920). As noted in the methods, PC3 and PC4 were both related to
²⁰⁴ the orientation of the copepod and the appendage visibility respectively (Sup-
²⁰⁵ plemental Figure 3).

²⁰⁶ The morphological groupings were assigned along PC1 as low, mid and high.
²⁰⁷ Then along PC2, groups were assigned within each PC1-group (Figure 1). To
²⁰⁸ confirm the morphospace grouping resulted in ecologically relevant categories,
²⁰⁹ the morphological groups were compared against known copepod metrics.
²¹⁰ Across all PC1-groups, there was a clear difference in feret diameter. The
²¹¹ median feret diameter of the low group was 1.97mm. The median feret diameter
²¹² of the mid and high groups were 2.84mm and 4.83mm, respectively (Figure 2A).
²¹³ All groups were significantly different from one another (Dunn Kruskall-Wallace
²¹⁴ test, $p < 0.001$). PC2 groups as a whole were also significantly different from
²¹⁵ one another (Dunn Krustall-wallace test, $p < 0.001$). However, within each
²¹⁶ PC2-group, there was a clear tendency for larger copepods (high PC1 group)

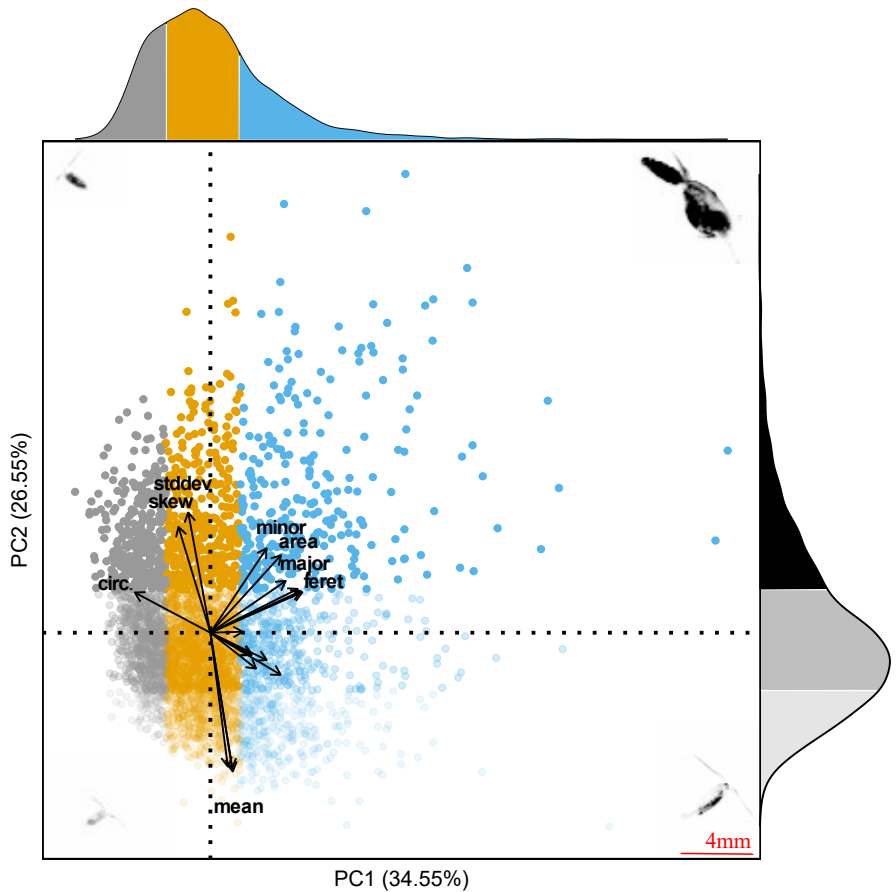


Figure 1: First two principal components of the morphospace. Proportion of variance explained by the two axis is 61.1%. Each point represents an individual copepod. The color and transparency of each point corresponds to the morphological groups based on percentile along each axis. Along PC1, grey corresponds to the low-group (<25th percentile), orange to the mid group (25th-75th percentiles), and blue to the high-group (75th percentile). Along PC2, low, mid, and high groups are distinguished by increasing opacity. Marginal distribution display the proportion of observations in each group. Representative vignettes of copepods are shown in the corners corresponding to their place in the morphospace. 4mm scale bar in the bottom right is shown for the vignettes.

²¹⁷ to be more transparent (Figure 2B).

²¹⁸ **4.2 Vertical Profiles of Morphological Groups**

²¹⁹ For all groups, the 20m-binned profiles show a notable structure. While cope-
²²⁰ pods were observed throughout the mesopelagic (Supplemental Figure 4), the
²²¹ majority of day/night differences were observed above 600m (Figure 3). For
²²² most morphological groups, there was a peak in nighttime concentration in the
²²³ lower epipelagic (50m-200m). Similarly, there was a decrease in average day-
²²⁴ time concentration over the same region. This pattern is particularly apparent
²²⁵ for the groups which are mid and high on both PCs (Figure 3B, C, E, F). Across
²²⁶ all groups, both average daytime and nighttime concentration were low in the
²²⁷ upper mesopelagic (200m-300m). Then, there was a peak in average daytime
²²⁸ concentration in the depth bins in the mid-mesopelagic (400m-600m).

²²⁹ **4.3 Weighted mean depth analysis**

²³⁰ The bin-constrained bootstrap approach provided a direct method to compare
²³¹ DVM between groups. Size (PC1) had a clear effect on DVM magnitude. First,
²³² for all PC1 groups, daytime WMD 95% bootstrapped confidence intervals (95%
²³³ CIs) were deeper and non-overlapping with the nighttime 95% CIs (Figure 4).
²³⁴ This indicates a clear DVM pattern. However, the differences in day and night
²³⁵ CIs varied between morphological groups. All PC1 groups had a similar, over-
²³⁶ lapping nighttime 95% CI in the lower epipelagic (~145m - ~200m). However,
²³⁷ there was a clear difference in the depth of the daytime 95% CIs. The small

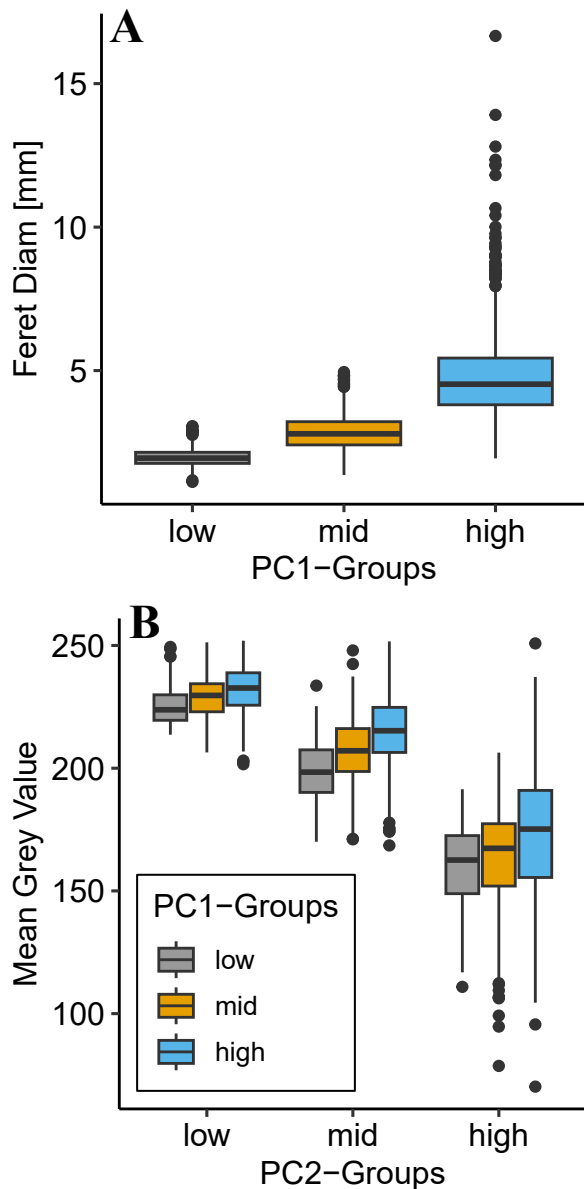


Figure 2: Comparison of morphological groups to relevant parameters. Groups were constructed along principal components with low as below 25th percentile, mid as 25th-50th percentile, and high as above 75th percentile. (A) PC1 groups are significantly different along feret diameter and display a clear trend for size. (B) PC2 groups are significantly different in terms of mean grey value. Note that a low mean grey value indicates a darker copepod.

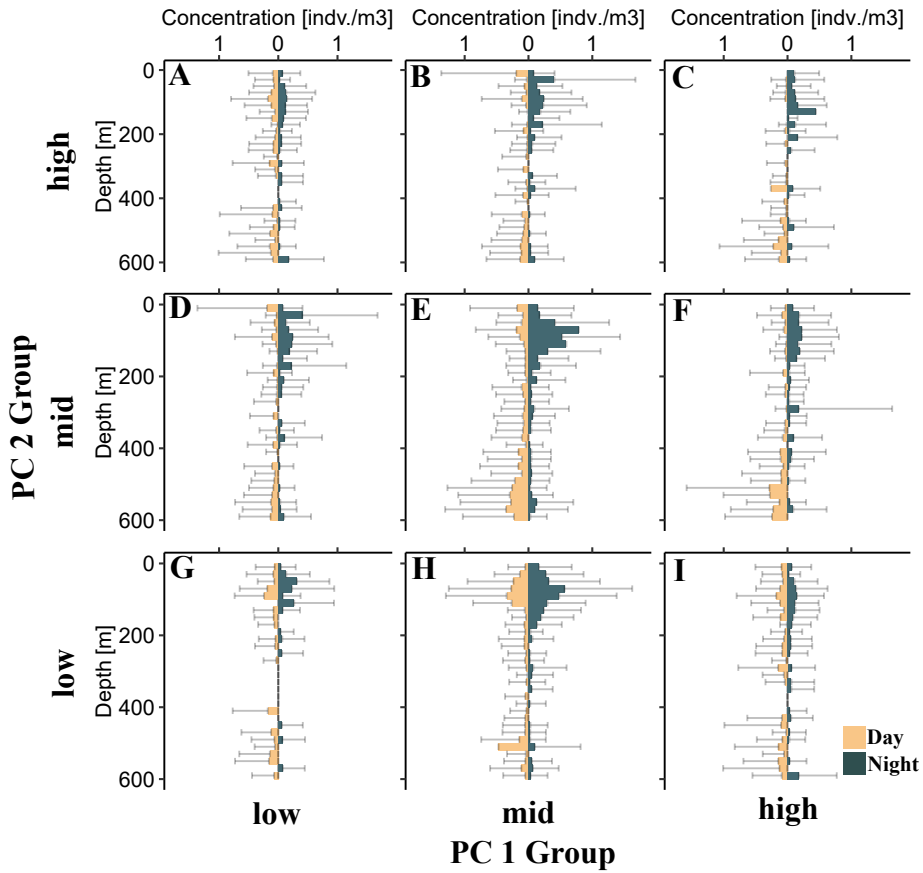


Figure 3: Average vertical profile of different copepod morphological groups. Bars display average concentration in a 20m depth bin. On each panel, left-side bars (tan) correspond to daytime while right-side (teal) bars correspond to nighttime. Standard deviation is shown for each 20m depth bin. Each panel corresponds to a morphological group along PC1 (size axis) and PC2 (transparency axis). (A) low PC1, high PC2; (B) mid PC1, high PC2; (C) high PC1, high PC2; (D) low PC1, mid PC2; (E) mid PC1, mid PC2; (F) high PC1, mid PC2; (G) low PC1, low PC2; (H) mid PC1, low PC2; (I) high PC1, low PC2

²³⁸ (low PC1) group had the shallowest 95% CI (235.2m-296.0m). The mid PC1
²³⁹ group's daytime 95% CI was slightly deeper (309.0m-347.3m). The large (high
²⁴⁰ PC1) group daytime 95% CI was even lower (352.3m-405.0m).

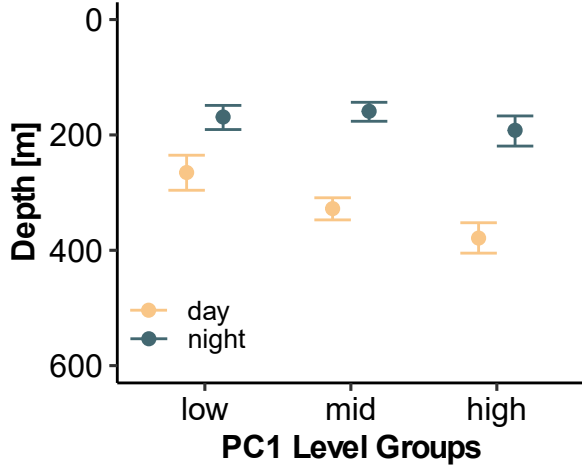


Figure 4: Mean bootstrapped weighted mean depth and 95% confidence intervals for copepods of different morphological groups. Low, mid, and high groups correspond to the different percentiles along PC1 from the morphospace. PC1 largely is explained by size metrics, with higher scores indicating a larger copepod.

²⁴¹ When considering the influence of transparency (PC2) on DVM magnitude, we
²⁴² compared PC2 groups within their PC1 grouping. This approach was warranted
²⁴³ because of the tendency for size to have a slight effect on transparency (Figure
²⁴⁴ 2). At this level of comparison, there were several notable trends. For the
²⁴⁵ smaller copepods (low PC1), once the data were split into PC2 groups, the
²⁴⁶ wider 95% CIs indicate little to no DVM signal. Generally, the daytime 95%
²⁴⁷ CIs and nighttime 95% CIs are overlapping or near-overlapping (Figure 5A).
²⁴⁸ With mid sized copepods, there was a clear DVM signal. However, all PC2
²⁴⁹ groups appeared to have a similar DVM magnitude with each group's daytime

250 95% CIs overlapping with each other (Figure 5B). There was a difference in
 251 DVM magnitude across PC2 groups within the largest copepods. The more
 252 transparent copepods (low PC2 group) showed no DVM signal, with a shallow
 253 daytime WMD. However, the darker copepods (mid and high PC2 groups) had
 254 deeper daytime WMDs (Figure 5c).

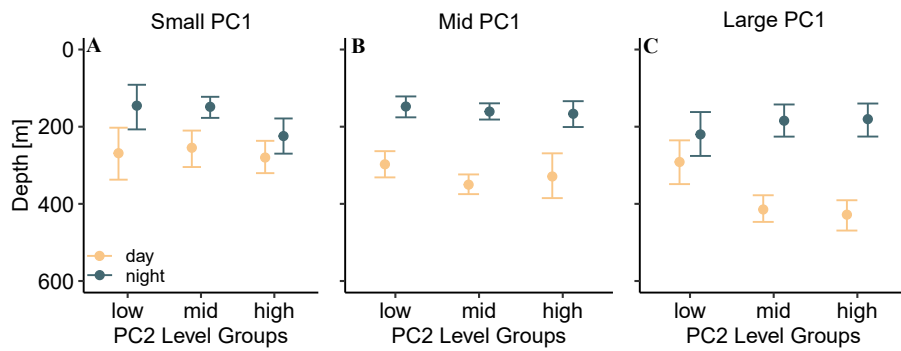


Figure 5: Mean bootstrapped weighted mean depth and 95% confidence intervals shown by copepod morphological groups along PC2 (transparency). Each panel represents a different size group of copepods (PC1 groups).

255 5 Discussion

256 5.1 Copepod morphospace

257 In this study, we built on methods for describing morphospaces from similar
 258 in-situ imaging studies (Vilgrain et al. 2021; Trudnowska et al. 2021; Sonnet
 259 et al. 2022). The PCA-defined morphospace with the present data aligns well
 260 with the prior applications. Interestingly, the proportion of morphological vari-
 261 ation explained by each axis in the morphospace defined on Arctic copepods by
 262 Vilgrain et al. (2021) is extremely similar to the morphospace axes in this study.

263 This similarity is striking considering the vastly different copepod community
264 compositions between the Arctic ocean and subtropical gyres (Soviadan et al.
265 2022). The similarity of morphospaces could also be an artifact of the similarity
266 of input data. Given the UVP has a limited range of observable size classes
267 (Picheral et al. 2010), only copepods above a certain size were fed into both
268 PCAs. Alternatively, the similarity of studies suggest that copepod morpholog-
269 ical variation might be well described by these two primary axes. (Sonnet et
270 al. 2022) used phytoplankton images to investigate how a morphospace could
271 be used to evaluate community composition changes over time. Comparisons
272 of copepod morphospaces across temporal and spatial scales may offer a useful
273 metric for answering biogeographic and ecological questions.

274 5.2 Morphology and DVM

275 The pattern of DVM described in this study is consistent with the general night-
276 time ascent DVM pattern (Bianchi and Mislan 2016; Bandara et al. 2021). The
277 average vertical profiles display a clear day/night difference (Figure 3). In each
278 20m depth bin, there was large variation, often exceeding the average concen-
279 tration. This large variation however, was expected. There can be consider-
280 able variation between UVP estimates of zooplankton abundance (Barth and
281 Stone 2022). Additionally, in this study we pooled casts across multiple seasons.
282 Variability in copepod DVM has been described across seasons (Whitmore and
283 Ohman 2021). While seasonal variability in DVM is an interesting question
284 in the Sargasso Sea, the nature of our dataset did not lend itself to this investi-

gation. However, despite the need to pool UVP casts across cruises, the signal of DVM was still observable. Previous studies using in-situ imaging have also noted a signal of DVM with copepods (Pan et al. 2018; Whitmore and Ohman 2021). Yet due to small and uneven sampling, it can be a challenge to quantify DVM using in-situ imaging. As presented in this paper, bin-constrained bootstrapping offers a robust method to quantify WMD and investigate DVM hypotheses.

Consistent with the size-based hypothesis (H1), we documented a clear effect in which larger copepods migrated further. This finding is consistent with several studies which have documented a size-dependent relationship for copepod DVM (Ohman and Romagnan 2016; Aarflot et al. 2019; Pinti et al. 2019). Ohman and Romagnan (2016) noted that moderate-size copepods had the largest migrations. While this may seem contradictory to the present study, the difference between study systems needs be taken into account. The copepods described in the large (high PC1) group had a mean feret diameter of nearly 5mm. Conversely, in Ohman and Romagnan (2016)'s study the "moderate" copepods ranged from 4mm-6mm.

The transparency-based hypothesis (H2) was only supported by patterns within the large copepod group. The large but more transparent copepods (low PC2, high PC1) did not have a detectable DVM signal. Yet the darker copepods (mid and high PC2) had a large DVM signal. Hays (2003) described that copepod pigmentation could explain increased DVM with small (<1 mm) copepods. The lack of a transparency effect for the mid- and low PC1 groups in our study is

surprising. One possibility is that the small, transparent copepods were not well sampled by the UVP (Figure 2). Alternatively, some copepods which do not migrate may have pigmentation to avoid damage from UV radiation. The grey-value recorded in UVP-imaged copepods can be indicative of many features beyond simply pigmentation, notably egg-sacs and gut contents (Vilgrain et al. 2021). Such characteristics vary much more between individuals and can have varied influences on DVM (PEARRE Jr. 2003). Thus the relationship between color and DVM is the result of a delicate balance of minimizing multiple ecological and biological risks (Hansson 2004; Hylander et al. 2014). While well documented, predator avoidance may not always be the primary selective pressure on copepod traits. For example, if the costs of migration are too large for some copepods, they will remain near the surface. However, these copepods then are exposed to UV light and may increase pigmentation to reduce damage.

5.3 Conclusion

Overall, our results reveal a complex dynamic between copepod traits and DVM behavior. This study provided new insight into the DVM dynamics in oligotrophic gyres. While many studies have established size as a major trait influencing DVM, investigations into other traits are more limited. Here, we show using in-situ imaging that color/transparency has a major role in DVM behavior, for some sizes of copepods. How size and color influence DVM across seasons and environmental conditions remains a major question. As plankton in-situ imaging tools are used more commonly by oceanographers, larger datasets will

³³⁰ facilitate new investigations.

³³¹ **6 Acknowledgements**

³³² Field work for this project was supported by the Bermuda Atlantic Time Series
³³³ Study through NSF OCE 1756105 & NSF OCE 1756312. We would also like
³³⁴ to thank the BATS research technicians, marine technicians, and crew of the
³³⁵ R/V Atlantic Explorer. Dr. Ryan Rykaczewski assisted with the initial set-up
³³⁶ of the UVP. Dr. Leo Blanco-Bercial and Dr. Amy Maas both valuable insight
³³⁷ and guidance on the analysis.

³³⁸ **6.1 References**

- ³³⁹ Aarflot, J. M., D. L. Aksnes, A. F. Opdal, H. R. Skjoldal, and Ø. Fiksen.
³⁴⁰ 2019. Caught in broad daylight: Topographic constraints of zooplankton depth distributions. Limnology and Oceanography **64**: 849–859.
³⁴¹ doi:[10.1002/limo.11079](https://doi.org/10.1002/limo.11079)
- ³⁴² Aksnes, D. L., and A. C. W. Utne. 1997. A revised model of visual range in fish. Sarsia **82**: 137–147. doi:[10.1080/00364827.1997.10413647](https://doi.org/10.1080/00364827.1997.10413647)
- ³⁴³ Archibald, K. M., D. A. Siegel, and S. C. Doney. 2019. Modeling the Impact of Zooplankton Diel Vertical Migration on the Carbon Export Flux of the Biological Pump. Global Biogeochemical Cycles **33**: 181–199.
³⁴⁴ doi:[10.1029/2018GB005983](https://doi.org/10.1029/2018GB005983)
- ³⁴⁵ Bandara, K., Ø. Varpe, L. Wijewardene, V. Tverberg, and K. Eiane. 2021. Two hundred years of zooplankton vertical migration research. Biological

- 351 Reviews **96**: 1547–1589. doi:[10.1111/brv.12715](https://doi.org/10.1111/brv.12715)
- 352 Barth, A., and J. Stone. 2022. Comparison of an in situ imaging device and
353 net-based method to study mesozooplankton communities in an oligotrophic
354 system. Frontiers in Marine Science **9**.
- 355 Bianchi, D., and K. a. S. Mislan. 2016. Global patterns of diel vertical migration
356 times and velocities from acoustic data. Limnology and Oceanography **61**:
357 353–364. doi:[10.1002/lno.10219](https://doi.org/10.1002/lno.10219)
- 358 Brierley, A. S. 2014. Diel vertical migration. Current Biology **24**: R1074–R1076.
359 doi:[10.1016/j.cub.2014.08.054](https://doi.org/10.1016/j.cub.2014.08.054)
- 360 Gorsky, G., M. D. Ohman, M. Picheral, and others. 2010. Digital zooplankton
361 image analysis using the ZooScan integrated system. Journal of Plankton
362 Research **32**: 285–303. doi:[10.1093/plankt/fbp124](https://doi.org/10.1093/plankt/fbp124)
- 363 Hansson, L.-A. 2004. Plasticity in Pigmentation Induced by Conflicting Threats
364 from Predation and Uv Radiation. Ecology **85**: 1005–1016. doi:[10.1890/02-0525](https://doi.org/10.1890/02-0525)
- 365 Hays, G. C. 2003. A review of the adaptive significance and ecosystem conse-
366 quences of zooplankton diel vertical migrations. Springer Netherlands. 163–
367 170.
- 368 Hays, G. C., C. A. Proctor, A. W. G. John, and A. J. Warner. 1994. Inter-
369 specific differences in the diel vertical migration of marine copepods: The
370 implications of size, color, and morphology. Limnology and Oceanography
371 **39**: 1621–1629. doi:[10.4319/lo.1994.39.7.1621](https://doi.org/10.4319/lo.1994.39.7.1621)
- 372 Hylander, S., J. C. Grenvald, and T. Kiørboe. 2014. Fitness costs and benefits

374 of ultraviolet radiation exposure in marine pelagic copepods. Functional
375 Ecology **28**: 149–158. doi:[10.1111/1365-2435.12159](https://doi.org/10.1111/1365-2435.12159)

376 Kelly, T. B., P. C. Davison, R. Goericke, M. R. Landry, M. D. Ohman, and M.
377 R. Stukel. 2019. [The importance of mesozooplankton diel vertical migration](#)
378 [for sustaining a mesopelagic food web](#). Frontiers in Marine Science **6**.

379 Maas, A. E., L. Blanco-Bercial, A. Lo, A. M. Tarrant, and E. Timmins-
380 Schiffman. 2018. Variations in copepod proteome and respiration rate in
381 association with diel vertical migration and circadian cycle. The Biological
382 Bulletin **235**: 30–42. doi:[10.1086/699219](https://doi.org/10.1086/699219)

383 Ohman, M. D. 2019. A sea of tentacles: optically discernible traits resolved from
384 planktonic organisms in situ H. Browman [ed.]. ICES Journal of Marine
385 Science **76**: 1959–1972. doi:[10.1093/icesjms/fsz184](https://doi.org/10.1093/icesjms/fsz184)

386 Ohman, M. D., and J.-B. Romagnan. 2016. Nonlinear effects of body size and
387 optical attenuation on Diel Vertical Migration by zooplankton. Limnology
388 and Oceanography **61**: 765–770. doi:[10.1002/limo.10251](https://doi.org/10.1002/limo.10251)

389 Ohman, M. D., J. A. Runge, E. G. Durbin, D. B. Field, and B. Niehoff.
390 2002. On birth and death in the sea. Hydrobiologia **480**: 55–68.
391 doi:[10.1023/A:1021228900786](https://doi.org/10.1023/A:1021228900786)

392 Pan, J., F. Cheng, and F. Yu. 2018. [The diel vertical migration of zooplankton](#)
393 [in the hypoxia area observed by video plankton recorder](#). IJMS Vol.47(07)
394 [July 2018].

395 PEARRE Jr., S. 2003. Eat and run? The hunger/satiation hypothesis in vertical
396 migration: history, evidence and consequences. Biological Reviews **78**: 1–79.

- 397 doi:[10.1017/S146479310200595X](https://doi.org/10.1017/S146479310200595X)
- 398 Picheral, M., S. Colin, and J.-O. Irisson. [EcoTaxa](#), a tool for the taxonomic
399 classification of images.
- 400 Picheral, M., L. Guidi, L. Stemmann, D. M. Karl, G. Iddaoud, and G. Gorsky.
401 2010. The Underwater Vision Profiler 5: An advanced instrument for high
402 spatial resolution studies of particle size spectra and zooplankton. Limnology
403 and Oceanography: Methods **8**: 462–473. doi:[10.4319/lom.2010.8.462](https://doi.org/10.4319/lom.2010.8.462)
- 404 Pinti, J., T. Kiørboe, U. H. Thygesen, and A. W. Visser. 2019. Trophic in-
405 teractions drive the emergence of diel vertical migration patterns: A game-
406 theoretic model of copepod communities. Proceedings of the Royal Society
407 B: Biological Sciences **286**: 20191645. doi:[10.1098/rspb.2019.1645](https://doi.org/10.1098/rspb.2019.1645)
- 408 Robison, B. H., R. E. Sherlock, K. R. Reisenbichler, and P. R. McGill. 2020.
409 [Running the gauntlet: Assessing the threats to vertical migrators](#). Frontiers
410 in Marine Science **7**.
- 411 Schnetzer, A., and D. K. Steinberg. 2002. Active transport of particu-
412 late organic carbon and nitrogen by vertically migrating zooplankton
413 in the Sargasso Sea. Marine Ecology Progress Series **234**: 71–84.
414 doi:[10.3354/meps234071](https://doi.org/10.3354/meps234071)
- 415 Siegel, D. A., T. DeVries, I. Cetinić, and K. M. Bisson. 2023. Quantifying
416 the ocean’s biological pump and its carbon cycle impacts on global scales.
417 Annual Review of Marine Science **15**: null. doi:[10.1146/annurev-marine-040722-115226](https://doi.org/10.1146/annurev-marine-040722-115226)
- 418
419 Sonnet, V., L. Guidi, C. B. Mouw, G. Puggioni, and S.-D. Ayata. 2022. Length,

420 width, shape regularity, and chain structure: time series analysis of phy-
421toplankton morphology from imagery. Limnology and Oceanography **67**:
422 1850–1864. doi:[10.1002/lno.12171](https://doi.org/10.1002/lno.12171)

423 Soviadan, Y. D., F. Benedetti, M. C. Brandão, and others. 2022.
424 Patterns of mesozooplankton community composition and vertical
425 fluxes in the global ocean. Progress in Oceanography **200**: 102717.
426 doi:[10.1016/j.pocean.2021.102717](https://doi.org/10.1016/j.pocean.2021.102717)

427 Steinberg, D. K., C. A. Carlson, N. R. Bates, S. A. Goldthwait, L. P. Madin,
428 and A. F. Michaels. 2000. Zooplankton vertical migration and the active
429 transport of dissolved organic and inorganic carbon in the Sargasso Sea.
430 Deep Sea Research Part I: Oceanographic Research Papers **47**: 137–158.
431 doi:[10.1016/S0967-0637\(99\)00052-7](https://doi.org/10.1016/S0967-0637(99)00052-7)

432 Steinberg, D. K., C. A. Carlson, N. R. Bates, R. J. Johnson, A. F. Michaels,
433 and A. H. Knap. 2001. Overview of the US JGOFS Bermuda Atlantic
434 Time-series Study (BATS): a decade-scale look at ocean biology and biogeo-
435 chemistry. Deep Sea Research Part II: Topical Studies in Oceanography **48**:
436 1405–1447. doi:[10.1016/S0967-0645\(00\)00148-X](https://doi.org/10.1016/S0967-0645(00)00148-X)

437 Steinberg, D. K., and M. R. Landry. 2017. Zooplankton and the ocean carbon
438 cycle. Annual Review of Marine Science **9**: 413–444. doi:[10.1146/annurev-marine-010814-015924](https://doi.org/10.1146/annurev-marine-010814-015924)

440 Trudnowska, E., L. Lacour, M. Ardyna, A. Rogge, J. O. Irisson, A. M. Waite, M.
441 Babin, and L. Stemmann. 2021. Marine snow morphology illuminates the
442 evolution of phytoplankton blooms and determines their subsequent vertical

443 export. *Nature Communications* **12**: 2816. doi:[10.1038/s41467-021-22994-4](https://doi.org/10.1038/s41467-021-22994-4)

444 Turner, J. 2004. The importance of small planktonic copepods and their roles

445 in pelagic marine food webs.,

446 Vilgrain, L., F. Maps, M. Picheral, M. Babin, C. Aubry, J.-O. Irisson, and S.-D.

447 Ayata. 2021. Trait-based approach using in situ copepod images reveals

448 contrasting ecological patterns across an Arctic ice melt zone. *Limnology*

449 and *Oceanography* **66**: 1155–1167. doi:[10.1002/lno.11672](https://doi.org/10.1002/lno.11672)

450 Whitmore, B. M., and M. D. Ohman. 2021. Zooglider-measured association of

451 zooplankton with the fine-scale vertical prey field. *Limnology and Oceanog-*

452 *raphy* **66**: 3811–3827. doi:[10.1002/lno.11920](https://doi.org/10.1002/lno.11920)

453 **7 Data availability statement**

454 All data used in this project are hosted on Ecopart ([https://ecopart.obs-vlfr.](https://ecopart.obs-vlfr.fr/)

455 [fr/](https://ecopart.obs-vlfr.fr/)). Data in its raw form can be accessed from their portal. However, all

456 summary and intermediate data products, as well as code, are publicly available

457 on GitHub (https://github.com/TheAlexBarth/DVM_Migration-Morphology).

458 Intermediate data products are formatted as R Data Structure objects, other

459 formats are available on request.

460 **8 Supplemental Information**

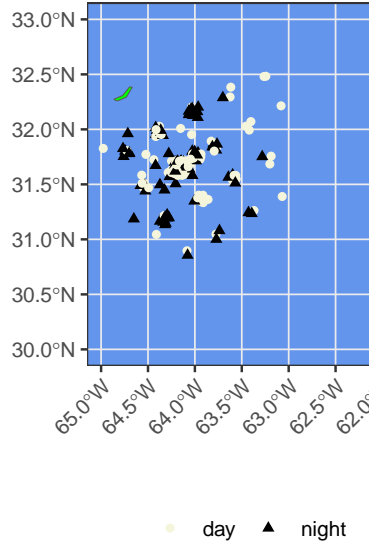


Figure 6: Supplemental Figure S1. Map of CTD Cast Deployments. Dark triangle points indicate night casts, tan circles indicate day casts.

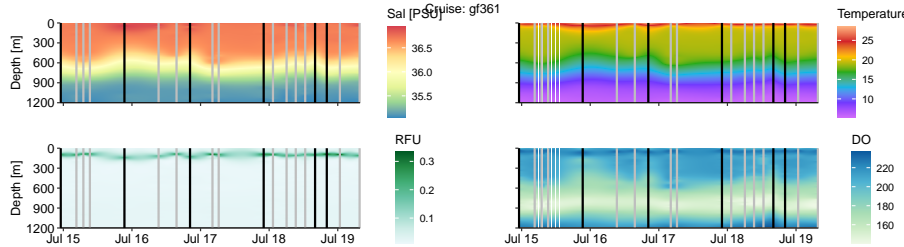


Figure 7: Supplemental Figure S2. Physical parameters across individual cruises. Vertical bars indicate CTD casts events with black indicating night and grey indicating day.

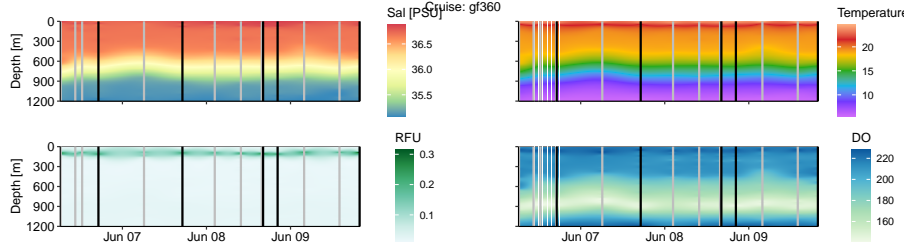


Figure 8: Supplemental Figure S2. Physical parameters across individual cruises. Vertical bars indicate CTD casts events with black indicating night and grey indicating day.

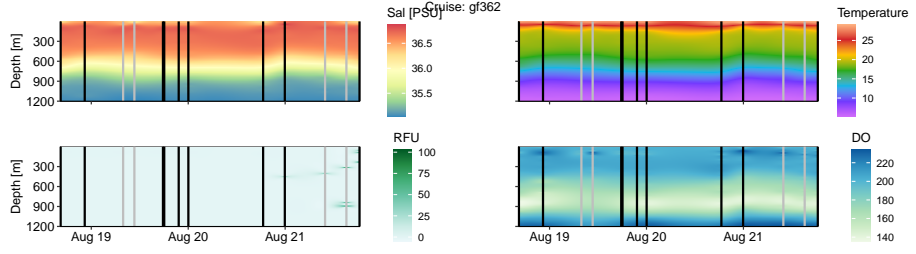


Figure 9: Supplemental Figure S2. Physical parameters across individual cruises. Vertical bars indicate CTD casts events with black indicating night and grey indicating day.

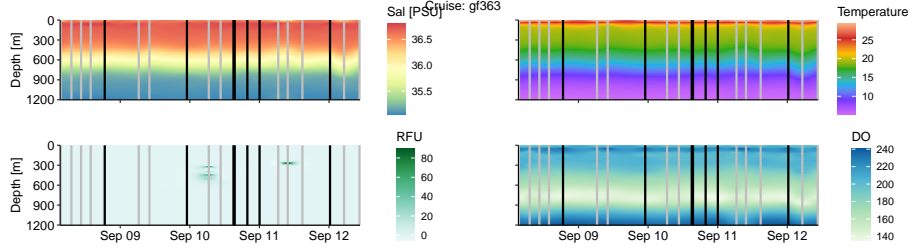


Figure 10: Supplemental Figure S2. Physical parameters across individual cruises. Vertical bars indicate CTD casts events with black indicating night and grey indicating day.

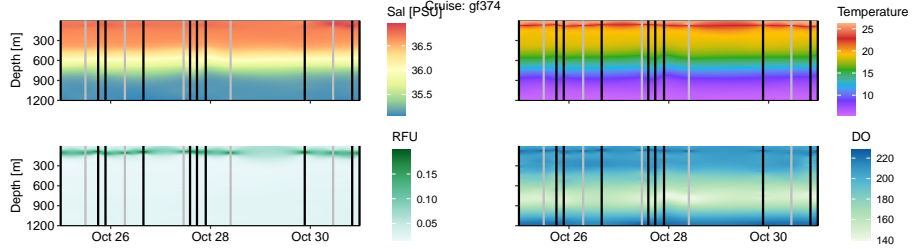


Figure 11: Supplemental Figure S2. Physical parameters across individual cruises. Vertical bars indicate CTD casts events with black indicating night and grey indicating day.

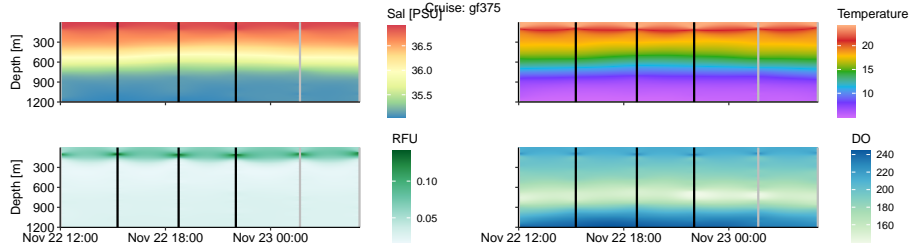


Figure 12: Supplemental Figure S2. Physical parameters across individual cruises. Vertical bars indicate CTD casts events with black indicating night and grey indicating day.

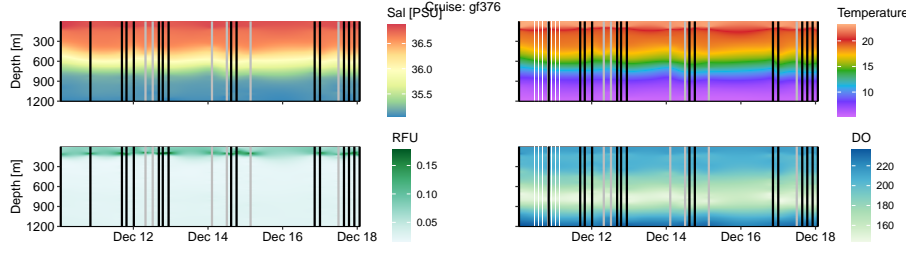


Figure 13: Supplemental Figure S2. Physical parameters across individual cruises. Vertical bars indicate CTD casts events with black indicating night and grey indicating day.

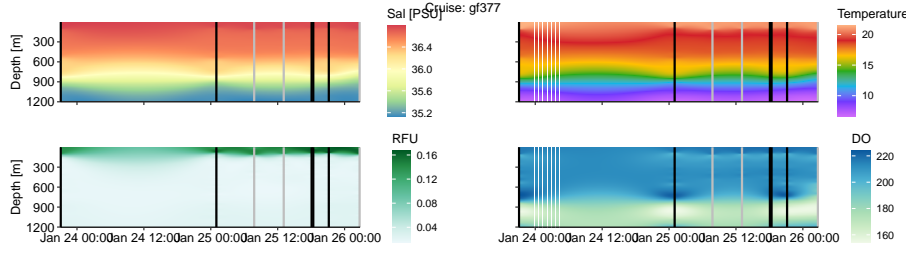


Figure 14: Supplemental Figure S2. Physical parameters across individual cruises. Vertical bars indicate CTD casts events with black indicating night and grey indicating day.

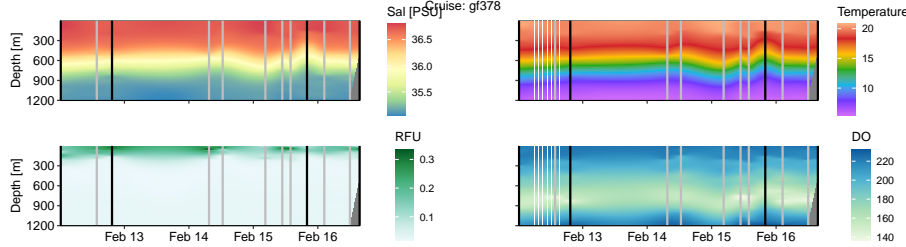


Figure 15: Supplemental Figure S2. Physical parameters across individual cruises. Vertical bars indicate CTD casts events with black indicating night and grey indicating day.

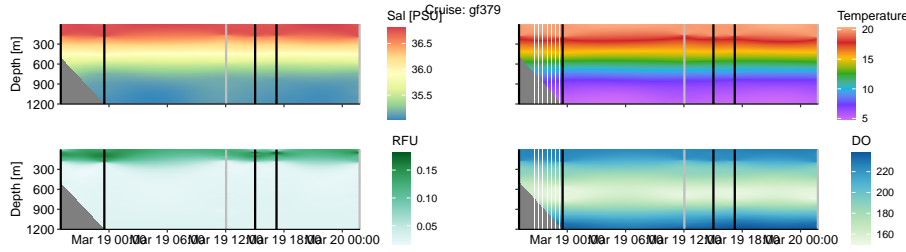


Figure 16: Supplemental Figure S2. Physical parameters across individual cruises. Vertical bars indicate CTD casts events with black indicating night and grey indicating day.

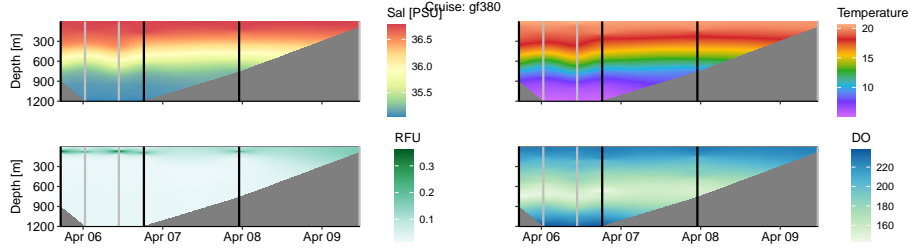


Figure 17: Supplemental Figure S2. Physical parameters across individual cruises. Vertical bars indicate CTD casts events with black indicating night and grey indicating day.

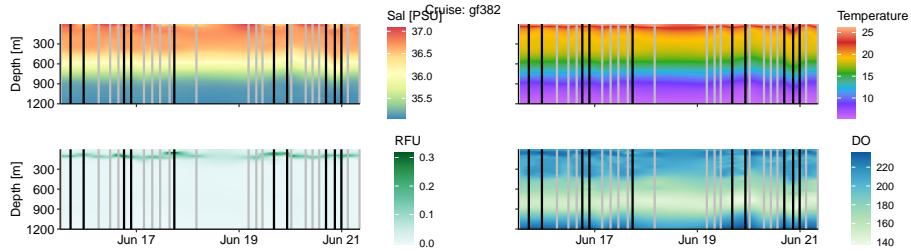


Figure 18: Supplemental Figure S2. Physical parameters across individual cruises. Vertical bars indicate CTD casts events with black indicating night and grey indicating day.

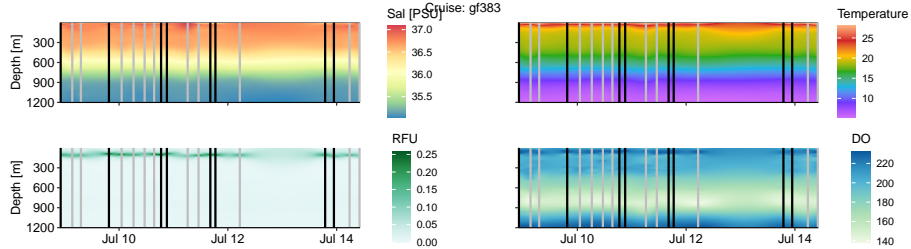


Figure 19: Supplemental Figure S2. Physical parameters across individual cruises. Vertical bars indicate CTD casts events with black indicating night and grey indicating day.

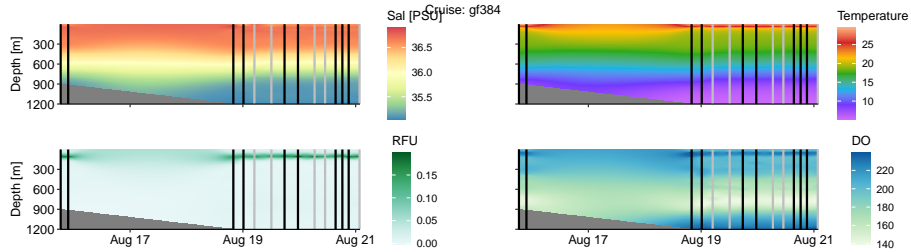


Figure 20: Supplemental Figure S2. Physical parameters across individual cruises. Vertical bars indicate CTD casts events with black indicating night and grey indicating day.

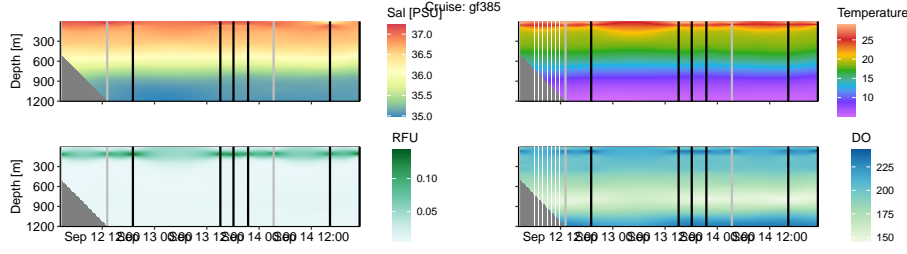


Figure 21: Supplemental Figure S2. Physical parameters across individual cruises. Vertical bars indicate CTD casts events with black indicating night and grey indicating day.

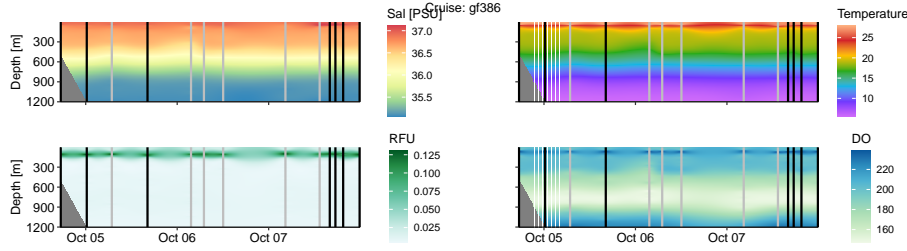


Figure 22: Supplemental Figure S2. Physical parameters across individual cruises. Vertical bars indicate CTD casts events with black indicating night and grey indicating day.

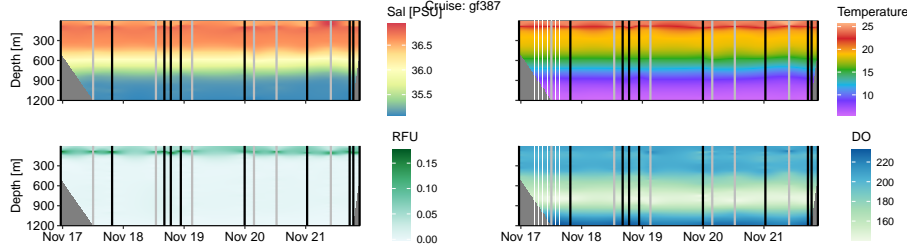


Figure 23: Supplemental Figure S2. Physical parameters across individual cruises. Vertical bars indicate CTD casts events with black indicating night and grey indicating day.

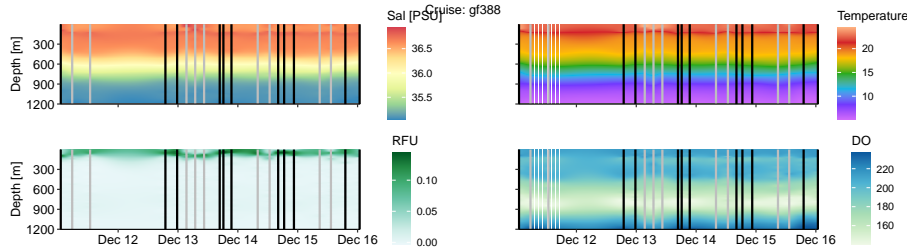


Figure 24: Supplemental Figure S2. Physical parameters across individual cruises. Vertical bars indicate CTD casts events with black indicating night and grey indicating day.

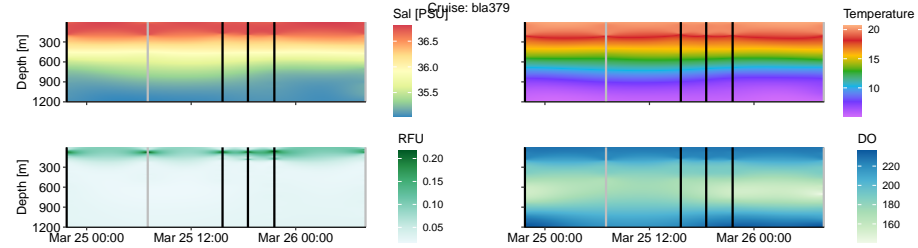


Figure 25: Supplemental Figure S2. Physical parameters across individual cruises. Vertical bars indicate CTD casts events with black indicating night and grey indicating day.

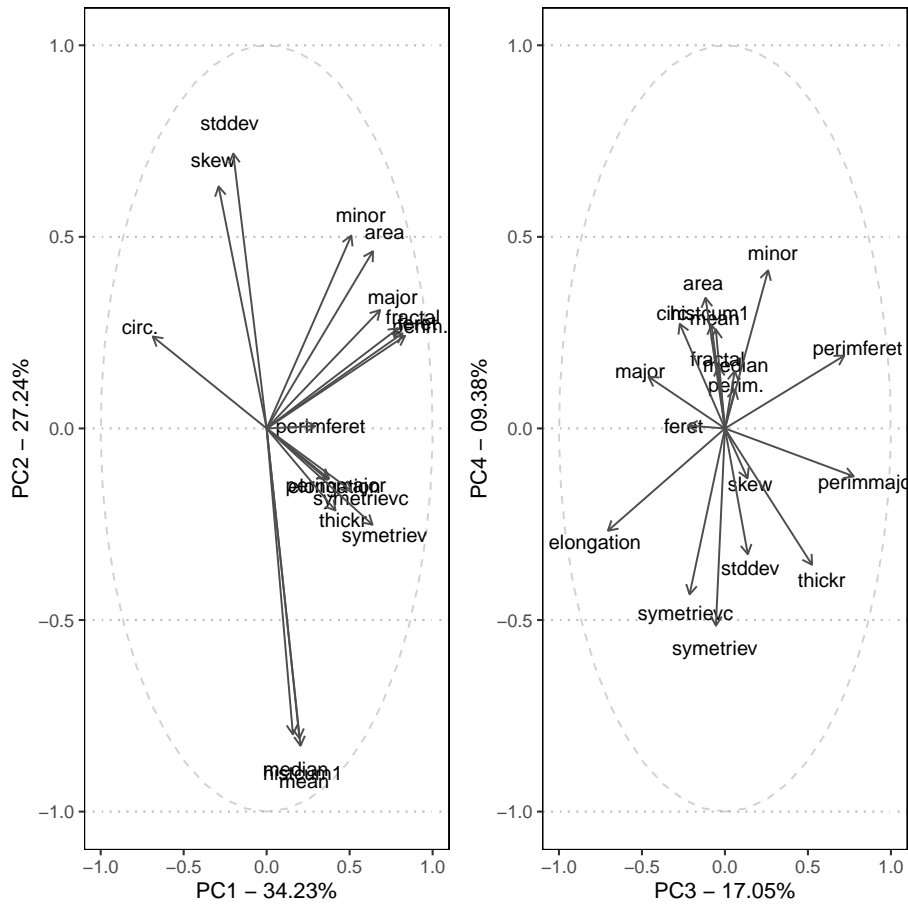


Figure 26: Supplemental Figure S3. PCA plot with major loading variables plotted.

	Dim.1	Dim.2	Dim.3	Dim.4
area	0.7115131	0.5137738	-0.1301928	0.3789753
circ.	-0.7627265	0.2665557	-0.3026239	0.3034329
elongation	0.4080632	-0.1487560	-0.7831847	-0.2965671
feret	0.9096148	0.2756948	-0.2479648	0.0082808
fractal	0.8816770	0.2904962	-0.0440580	0.1793785
histcum1	0.2197180	-0.8987922	-0.0901744	0.3005361
major	0.7593652	0.3432489	-0.5115438	0.1498407
mean	0.2266145	-0.9201880	-0.0611832	0.2875560
median	0.1758116	-0.8872673	0.0657406	0.1668198
minor	0.5668215	0.5593596	0.2891461	0.4585166
perim.	0.9268957	0.2685898	0.0681774	0.1135716
perimferet	0.3251295	0.0068372	0.7989292	0.2111105
perimmajor	0.4183142	-0.1460583	0.8627707	-0.1389696
skew	-0.3216781	0.7017490	0.1514517	-0.1447764
stddev	-0.2234641	0.7971849	0.1531288	-0.3647663
symetriev	0.7091737	-0.2793593	-0.0605051	-0.5720602
symetrievc	0.5673730	-0.1807542	-0.2368157	-0.4811256
thickr	0.4609473	-0.2379533	0.5832035	-0.3954358

⁴⁶¹ Supplemental Table S2. Loading scores for morphological factors on the PCA.